Karlsruhe Institute of Technology

Experimental calibration for DCDC specimens

P. Hettich, P. Zielonka, S. Fünfschilling,
K. G. Schell, S. Wagner, T. Fett

KIT SCIENTIFIC WORKING PAPERS 116

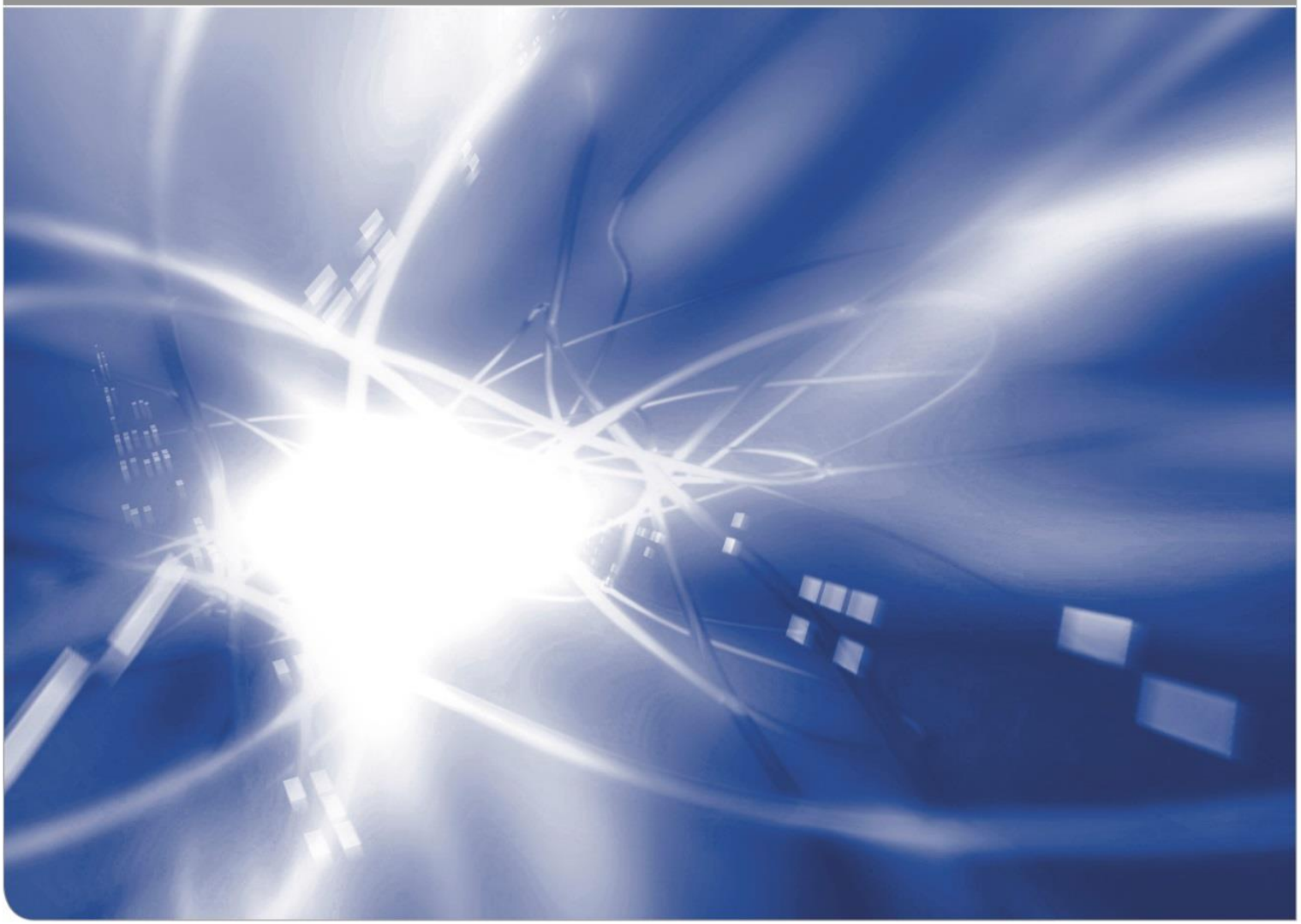

Karlsruhe Institute of Technology (KIT), Institute for Applied Materials
Karlsruhe, Germany

Impressum

Karlsruher Institut für Technologie (KIT)
www.kit.edu

2019

ISSN: 2194-1629

Abstract

The main advantages of DCDC-specimens are their completely stable crack extension properties and very high path stability due to the strongly negative T-stress term.

Unfortunately, problems of DCDC tests can be identified by comparing experimental results that show for different materials (silicon nitride, glass) deviations from the results to be expected by 2-dimensional FE modelling as usual done in literature.

Experimental calibrations on silicon nitrides and mixtures of silicon nitride and silicon carbide resulted in modified relations deviating from FE-results in literature.

As a possible source for the differences of measurements and 2-D-FE results, we identified the influence of Poisson's number. This parameter obviously causes deviations between *straight-crack assumption* in FE-modelling and observable curved crack fronts in the experiments.

In order to avoid specimen buckling we also used short specimens of roughly half length. This may slightly affect the stress intensity factors.

Contents

1. Introduction

The "double cleavage drilled compression" (DCDC) specimen is a rectangular bar with a circular hole in its centre that is loaded by compressive stresses p at the end faces (Fig. 1). The main advantages of DCDC-specimens, responsible for increasing popularity, are the completely stable crack extension after spontaneous crack initiation due to the decreasing stress intensity factor with increasing crack length and a very high path stability due to the strongly negative T-stress term. This specimen, predominantly applied to glasses and polymers can for instance be used for high-strength materials as silicon nitrides and should allow R-curve measurements $K_R(\Delta a)$ over large crack extensions Δa.

The most popular 2D stress intensity factor was determined by He et al. [1] via FE with the result of

$$K = \sigma\sqrt{\pi R}\, F(\tfrac{a}{R}, \tfrac{H}{R}), \quad \frac{1}{F(\frac{a}{R}, \frac{H}{R})} = \left(\frac{H}{R} + \left[0.235\frac{H}{R} - 0.259 \right] \frac{a}{R} \right) \tag{1a}$$

valid for $a \geq H$ (see also [2, 3]).

Extensive 2D-FE-computations were carried out by Pallares et al. [4] expressed similar to eq.(1a) with quadratic terms in H/R included

$$\frac{1}{F(\frac{a}{R}, \frac{H}{R})} = \left[c_0 + c_1\frac{H}{R} + c_2\left(\frac{H}{R}\right)^2 \right] + \left[c_3 + c_4\frac{H}{R} + c_5\left(\frac{H}{R}\right)^2 \right] \frac{a}{R} \tag{1b}$$

with the coefficients: c_0 =0.3156, c_1 =0.7350, c_2 =0.0346, c_3 = -0.4093, c_4 =0.3794, c_5= -0.0257. This relation is limited by $H/R < a/R < L/R - 2H/R$. In the following considerations we will use eq.(1b) as the actually best FE-solution.

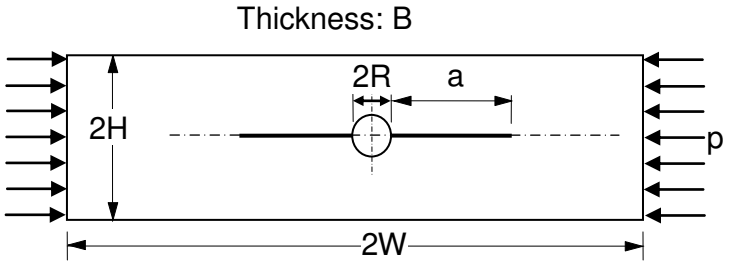

Fig. 1 The DCDC specimen (geometric data).

There are several problems in using the standard solution, eq.(1):

- Stress intensity factor solutions for the DCDC specimen are available in literature for the case of straight crack fronts, i.e. for 2dimensional problems. Real crack fronts are of course never straight apart from the hypothetic case of a material with Poisson ratio of ν=0.
- Finite Element programs are usually applied to linear problems, where the result is proportional to the applied loads. In the DCDC-specimen this linearity is violated especially for long cracks as has been stated by Plaisted et al. [5] and Nielsen et al.

[6]. These authors observed large COD at the crack mouth; therefore, they didn't use the solution by He et al. [1]. The stress intensity factor was obtained by performing FE computations directly for the experimentally observed loads.

- Moreover, with the high forces for silicon nitrides and the usual slender samples, there is a high risk of buckling. Therefore, we decided to use shorter samples for very high loading and to perform experimental calibrations on them that include the effect of crack-front curvature automatically.

2. Experimental calibration

2.1 Tested materials

The materials tested were a hot isostatically-pressed silicon nitride with 8.5 wt% Lu_2O_3 and 1.93 wt% MgO (denoted as MgLu), a silicon nitride ceramic with 2 wt% MgO and 5 wt% Y_2O_3 (material MgY), and commercial silicon nitrides with Y_2O_3 and Al_2O_3 content ((1) SL200 BG from CeramTec, Plochingen, Germany, (2) from Sumitomo, Japan). These materials were chosen since they showed constant crack resistance K_R already after 250 µm crack extension as can be concluded from R-curves in [7,8]. Figure 2 represents the R-curves obtained by measurements on edge-notched bending bars. The plateau values of these R-curves $K_{R,max}$ have to be interpreted as the fracture toughness K_{Ic} for toughness tests with the SEVNB-specimen (Single Edge Vee-Notched Beam). These values are compiled in Table 1.

In addition we carried out DCDC-measurements on SN-ceramics containing different portions of SiC (0, 10, 20, 30, 40, and 100 vol%).

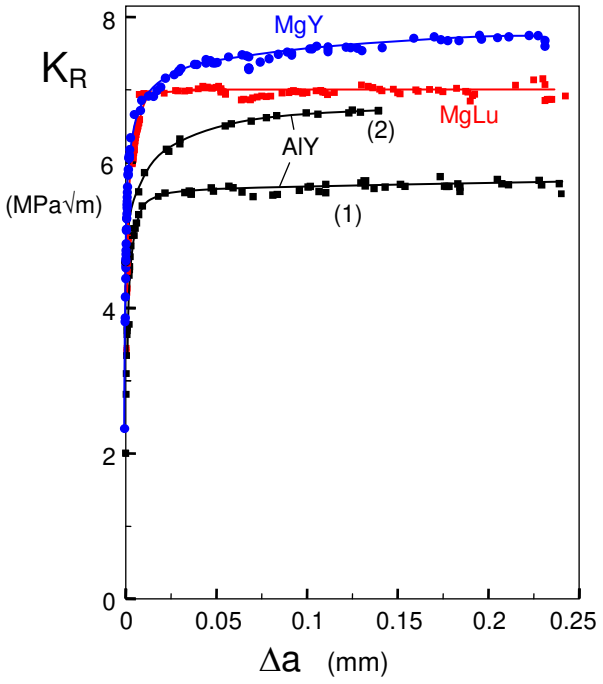

Fig. 2 R-curves for three silicon nitrides measured with edge-notched bending bars [7,8]. Results for silicon nitrides containing MgO+Lu_2O_3, MgO+Y_2O_3, and two Y_2O_3+Al_2O_3 ceramics (1: CeramTec, Plochingen, 2: Sumimoto, Japan).

Material	K_{Ic}
MgY-SN	7.7 MPa√m
MgLu-SN	7.0 MPa√m
AlY (1)	5.7 MPa√m
AlY (2)	6.7 MPa√m

Table 1 Toughness data from bending tests.

Measurements on glass were performed on a soda-borosilicate glass by Cai et al. [9] and on fused silica by Michalske et al. [10], both of "standard size" W/H=10. Since the applied loads were not reported by Cai et al. [9], we dealt predominantly with the data by Michalske et al. [10].

2.2 Curved crack contour and effective crack length

In-situ measurements on non-transparent materials as for instance silicon nitride provide the actual location where the crack terminates the surface. A crack surface is shown in Fig. 3a including an additional crack front marked by cyclic loading at a reduced upper stress level. Since the crack front is curved (see Fig. 3a), the measurement at the surface is not necessarily equivalent to the length of the straight crack, needed in eq.(1). This crack length denoted as a_1 is indicated in Fig. 3b. Figure 3c shows markings on a fractured surface of soda-lime glass obtained by partial unloading in subcritical crack growth tests. In measurements on glass and PMMA, the crack length is identified with the length a_2 as is present in the specimen centre. Using energy release rate considerations, the length of the related 2-dimensional crack would be that for a straight crack showing the same area as the curved one. The distance h is shown in Fig. 3d as a function of Poisson's ratio ν.

For the crack front described by a part of circle, the area S results from elementary geometry as

$$S = \tfrac{1}{8}\left(h + \frac{B^2}{4h}\right)^2\left(4\arctan\left[\frac{2h}{B}\right] - \sin\left[4\arctan\left[\frac{2h}{B}\right]\right]\right) = \tfrac{2}{3}Bh + O(h^3) \qquad (2)$$

Consequently, the related crack length is

$$a = a_1 + \Delta a; \quad \Delta a = S/B = \tfrac{2}{3}h \qquad (3a)$$

with $\boldsymbol{h \cong 0.35}$ **mm** for the crack in the SN-ceramic, Fig. 3a. Curve fitting of the data in Fig. 3d gives under the assumption of self-similar crack fronts

$$\frac{h}{B} \cong 0.155\nu + 0.548\nu^2 \qquad (3b)$$

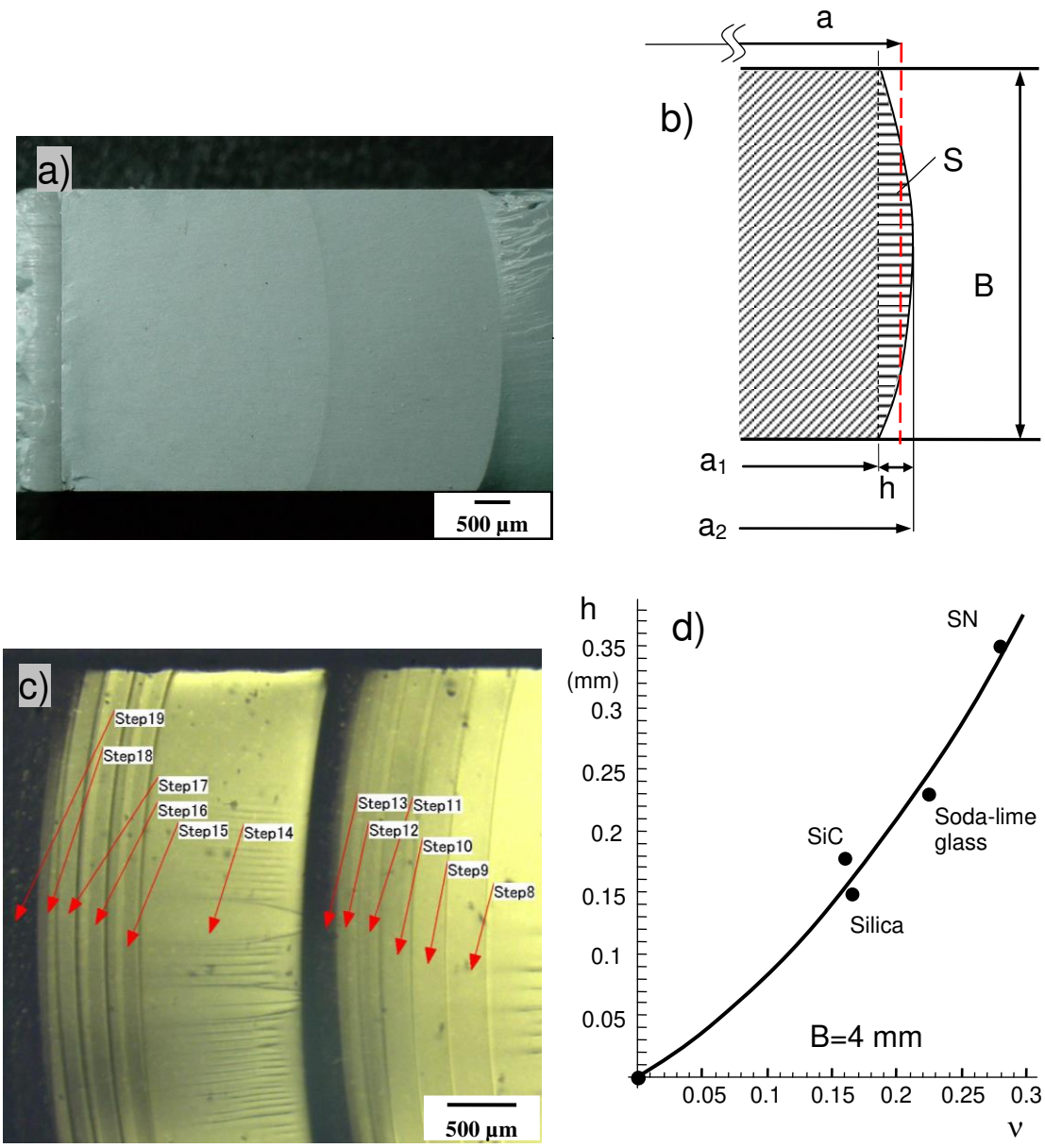

Fig. 3 a) Curved crack fronts in SN, first front marked by cyclic unloading, b) curved crack front replaced by a straight effective crack (dashed red line), c) crack fronts in soda-lime glass obtained in subcritical crack growth tests by partial unloading, d) length *h* of Fig. 3b versus Poisson's ratio ν.

2.3 Experimental results

The relevant specimen data are compiled in Table 2. The Young's modulus was determined by measuring the resonance frequency. Poisson's ratio for the SN-SiC materials was computed by application of the linear mixing rule with ν=0.28 for the SN and ν=0.16 for SiC.

The results from [10], directly compiled in form of a Table, are shown in Fig. 4c as the product of end-face pressures $p=|\sigma|$ and $\sqrt{R}$. Linear fitting of the linear parts of the dependency in the range of $3<a/R<10$ by

$$|\sigma|\sqrt{R} = A_1 + A_2 \frac{a}{R} \tag{4a}$$

results in the parameters A_1 and A_2 of Table 3.

Material	$B/(2H)$	R (mm)	H/R	E (GPa)	ν
Silica	0.867	1	3.75	69	0.16
Borosilicate glass	0.587	0.795	3.75	62.8	0.20
MgY-SN	0.816	0.522	3.21	320	0.28
MgLu-SN	0.705	0.530	3.81	320	0.28
AlY (2)	0.852	0.540	3.23	320	0.28
SN+0% SiC	0.953	0.485	4.11	303	0.28
SN+10% SiC	0.992	0.527	3.78	308	≈0.272
SN+20% SiC	0.992	0.520	3.80	319	≈0.264
SN+30% SiC	0.981	0.537	3.72	331	≈0.256
SN+40% SiC	0.979	0.521	3.81	327	≈0.248
SiC	0.830	0.538	3.70	411	0.16

Table 2 Data for DCDC-specimens.

Material	$A_1=(\lvert\sigma\rvert\sqrt{R})_{a\to 0}$ (MPa√m)	Slope A_2 (MPa√m)	$K_{Ic,meaured}$ (MPa√m)	K_{Ic} eq.(6a) (MPa√m)	K_{Ic} eq.(6b) (MPa√m)
Silica	1.62	0.246	0.74	0.766	0.807
MgY-SN	12.47	1.451	7.7	6.89	7.29
MgLu-SN	14.42	1.634	7.0	6.71	7.06
AlY (2)	11.7	1.253	6.7	6.42	6.80
SN	11.59	1.319	-	5.00	5.24
SN+10% SiC	10.23	1.191	-	4.80	5.05
SN+20% SiC	11.30	1.274	-	5.27	5.55
SN+30% SiC	11.23	1.14	-	5.35	5.64
SN+40% SiC	9.95	1.165	-	4.63	4.87
SiC	4.93	0.675	-	2.36	2.49

Table 3 Results from Figs. 4a-4c and fracture toughness from eq.(6a) and eq.(6b).

For the Si_3N_4 materials, we used specimens with the dimensions 2W=40 mm, H=2 mm, B=4 mm and $R\cong 0.5$ mm. For high loads we used short specimens with dimensions $2W$=25 mm, H=1.6-2 mm, $R\cong 0.5$ mm, and $B\cong 3$ mm in order to avoid any possible buckling effect. During load application the crack length was measured at the side surface using an optical microscope with large focal length. From these data, the effective length was determined via eq.(3). Results are plotted in Fig. 4b. Figure 4c represents results for the SN-SiC-ceramics. For a first comparison, the result obtained on short DCDC-specimens of MgLu-SN at a comparable value of H/R=3.8, is plotted in Fig. 5a as the red circles. Although these data differ strongly in slope, the straight parts of the data show the same extrapolated value at the origin, a=0.

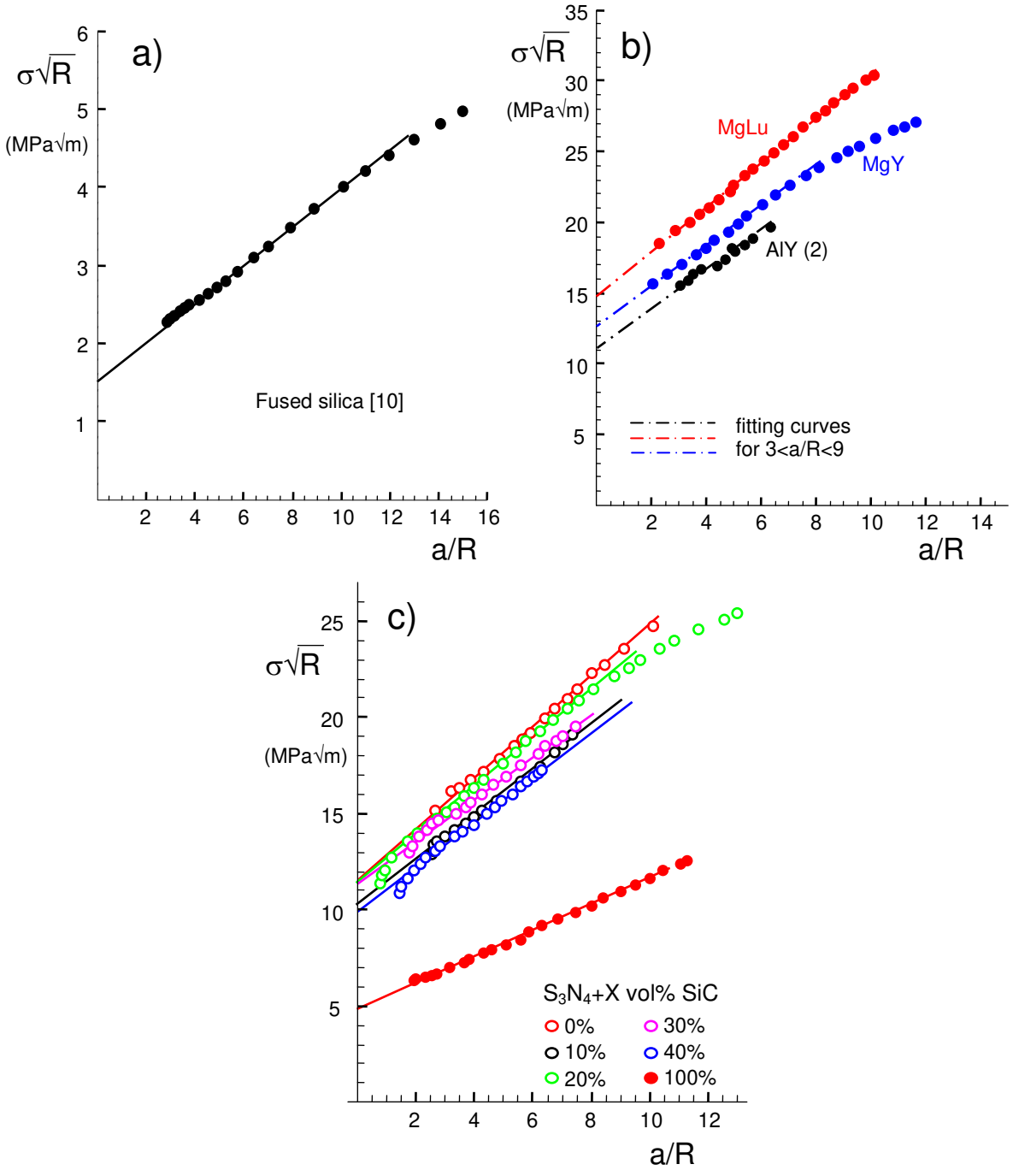

Fig. 4 Applied end-face pressure times $\sqrt{R}$ vs normalized crack length.

2.4 Normalized stress intensity factor and toughness

In literature the geometric function is sometimes determined experimentally, e.g. [9] and [10] for glasses, with known fracture toughness K_{Ic} by using the so-called normalized toughness K_{norm}

$$K_{norm} = \frac{K_{\mathrm{Ic}}}{p\sqrt{R}} \tag{5}$$

because this ratio represents the function $F(a/R,H/R)$ apart from the constant factor $\sqrt{\pi}$. Plotting the reciprocal normalized stress intensity factor versus a/R results in nearly

linear plots. The dash-dotted line in Fig. 5a represents eq.(1a) and the solid line eq.(1b) both plotted for H/R=3.75. The ordinate of Figs. 5a, 5b and 5c is given in terms of the reciprocal "normalized toughness" $1/K_{norm}$. The values of K_{norm} at a/R=0 agree very well with $1/(F\sqrt{\pi})$ from eq.(1b), as shown by the squares. Sufficient agreement is also visible for the eq.(1a) as indicated by the triangles. The dependencies $1/K_{norm}$ (a/R) are sufficiently linear only for $a/R \leq 10$.

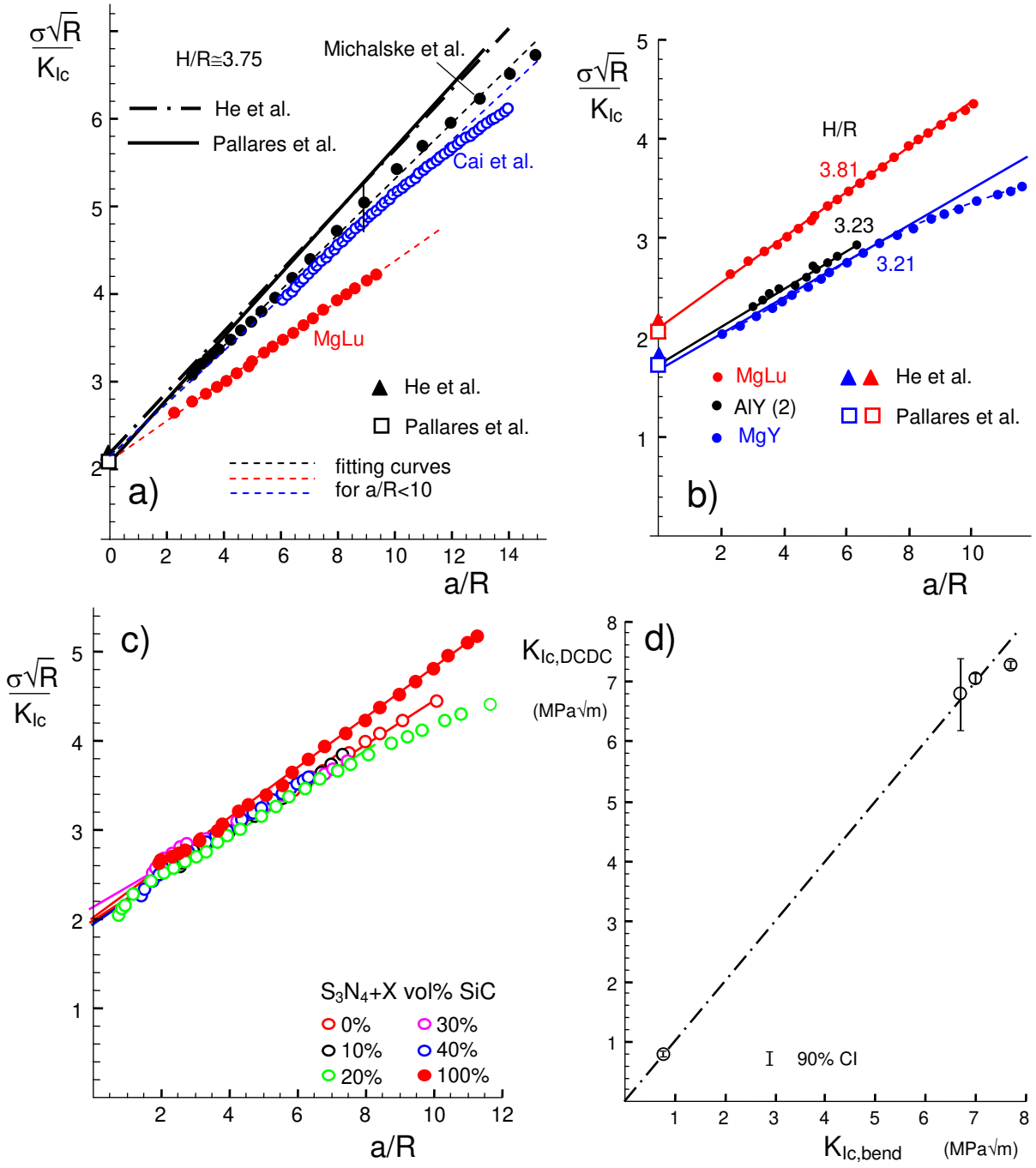

Fig. 5 a) Reciprocal normalized toughness vs. normalized crack length a/R from DCDC-tests for H/R≅3.75; Glasses from literature (blue and black), SN (red); b) results on SN-materials with different ratios of H/R, c) SN-ceramics with varying SiC content, d) fracture toughness K_{Ic} from eq.(6b) compared with measurements from bending tests.

For longer cracks the measured data deviate from the initial linear behaviour. This can be seen for the glasses and the MgY-SN that already deviates for $a/R>8$. From the conclusions by Plaisted et al. [5] and Nielsen et al. [6] the deviations of real K-values from FE-results should disappear for small crack extensions. Therefore, the values extrapolated to $a/R\rightarrow 0$ should match the FE-solution.
Similar to eq.(4a), we can express the straight lines in Figs. 5a-5d by

$$\frac{|\sigma|\sqrt{R}}{K_{Ic}} = B_1 + B_2 \frac{a}{R} \tag{4b}$$

with the toughness from Column 5 in Table 3.
The fracture toughness K_{Ic} may be obtained from eq.(1a) as

$$K_{Ic} = A_1 \sqrt{\pi} \frac{R}{H} \tag{6a}$$

and via eq.(1b)

$$K_{Ic} = \frac{A_1 \sqrt{\pi}}{c_0 + c_1 \frac{H}{R} + c_2 \left(\frac{H}{R} \right)^2} \tag{6b}$$

Results of both equations are given in Table 3.
A comparison with measured toughness data is shown in Fig. 5d. In this plot the toughness computed from the DCDC-data is plotted versus the results from Fig. 2 and data from [10]. The dashed-dotted line suggests $K_{\mathrm{Ic,DCDC}}=K_{\mathrm{Ic,bend}}$.

Material	Slope B_2 (experimental)	Slope B_2 Eq.(1b)	Slope ratio ≡ C Column 2/Column 3
MgY-SN	0.199	0.307	0.648
MgLu-SN	0.231	0.374	0.618
AlY (2)	0.184	0.309	0.595
SN	0.255	0.404	0.631
SN+10% SiC	0.243	0.371	0.655
SN+20% SiC	0.228	0.373	0.611
SN+30% SiC	0.202	0.365	0.554
SN+40% SiC	0.242	0.374	0.647
SiC	0.271	0.363	0.748

Table 4 Slopes of the reciprocal normalized toughness for $a/R\leq 8$, K_{Ic} from eq.(6b).

From Table 4 it can be seen that the slopes of the reciprocal normalized stress intensity factors, Fig. 5, deviate from the FE results for large cracks. At low loads as appear for the tests on glasses, the experimental slopes deviate by about 15% from the theoretical results. The deviations are clearly larger at high loads, namely

$$\frac{Slope_{\text{exper}}}{Slope_{\text{FE}}} \equiv C \approx 0.63 \;\; (0.018\; SD) \tag{7}$$

(Standard Deviation *SD* in parentheses). Based on the results in Table 4, we suggest use of the geometric function

$$\frac{1}{F(\frac{a}{R},\frac{H}{R})} = \left[c_0 + c_1\frac{H}{R} + c_2\left(\frac{H}{R}\right)^2\right] + C\left[c_3 + c_4\frac{H}{R} + c_5\left(\frac{H}{R}\right)^2\right]\frac{a}{R} \tag{8}$$

with the coefficients of eq.(1b). If the solution by He et al. [1] is preferred because of its popularity and simpler expression, we suggest

$$\frac{1}{F(\frac{a}{R},\frac{H}{R})} = \left(\frac{H}{R} + C\left[0.235\frac{H}{R} - 0.259\right]\frac{a}{R}\right) \tag{9}$$

The crack resistance curves for the silicon nitrides, computed via eqs.(8) and (9) are shown in Fig. 6 as the circles. The deviation from the horizontal indicate the effect of the curved results in Fig. 4b. The dash-dotted lines represent the toughness computed from eq.(6a) and (6b).

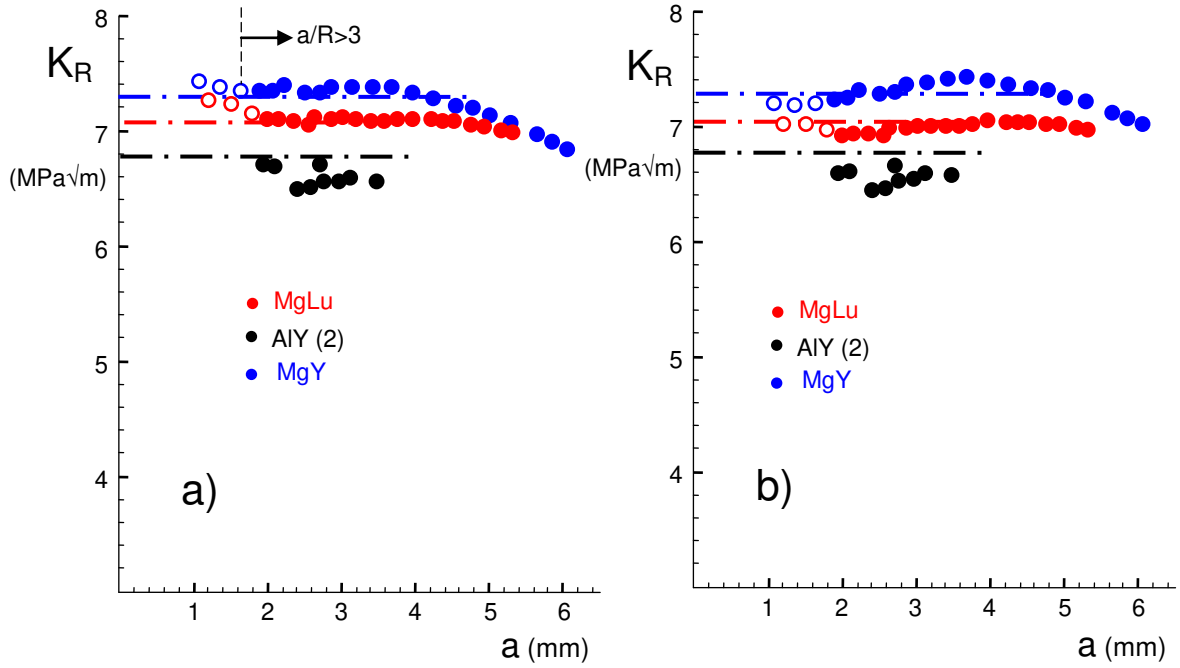

Fig. 6 Crack resistance curves for silicon nitrides (circles) and K_{Ic} from Table 3 (dash-dotted lines), a) evaluation via eq.(8), b) evaluation via eq.(9).

3. Influence of Poisson's number

Finite Element computations are usually performed for straight cracks under plain stress or plain strain conditions, assuming a 2-dimensional problem. Whereas plain stress and strain conditions result in the same stress intensity factor solution, the crack

front is curved for a 3-dimensional problem yielding deviating stress intensity factors. In the general case, ν≠0, the crack terminating angle φ (insert in Fig. 7) is [11]

$$\varphi \cong 90° - 38.8°\nu \tag{10}$$

Only for a hypothetical material with a Poisson number ν=0 the crack front would be straight even in the 3-dimensional case.
Therefore we plotted in Fig. 7 the slope ratio *C* in Table 4 versus the Poisson number ν. The correlation may be described by the linear expression

$$C \cong 1 - 1.37\nu \tag{11}$$

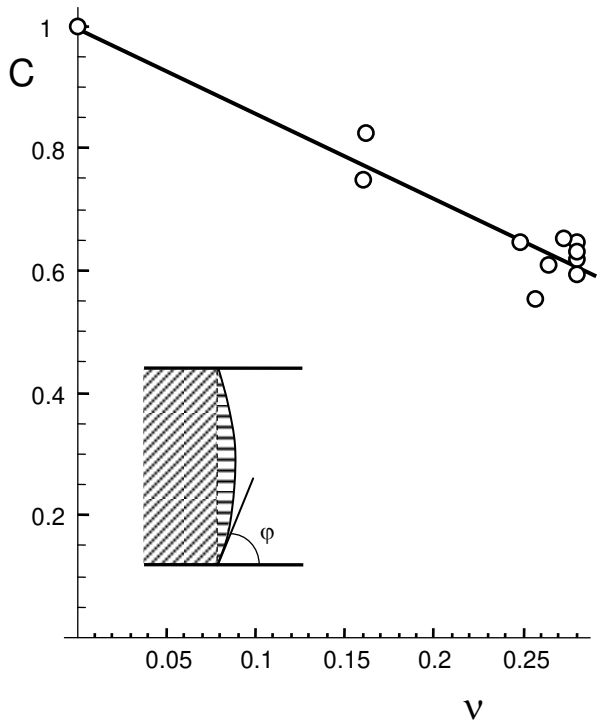

Fig. 7 Slope ratio *C* as a function of Poisson's number; straight line fit by eq.(11), insert: crack terminating angle.

4 Nonlinearity effect

Finite Element programs are usually applied to linear problems, where the result is proportional to the applied loads. Linear means in this case, that application of twice the load, the stresses in the body increase also by a factor of 2. When a tensile load is applied to a structure, linearity ensures that the stresses remain constant and only change their sign under compression loading. In the DCDC-specimen this linearity is violated.
The problem is schematically illustrated in Fig. 8. The mechanical problem of the estimation of the bending moment M_b, caused by the pressure force *F* in the internally notched bar, Fig. 8a, can be transformed into the equivalent problem of a notched bar

of length a with rigidly clamped ends. Figure 8b shows the left part of the specimen with length a. In Fig. 8c the pressure distribution is replaced by a single force in the distance b from the line in which the force at the ends is acting

$$b = \frac{\int \sigma(x)\, x dx}{\int \sigma(x)\, dx} \tag{12}$$

where x stands for the distance from the line in which the end forces act. A first approximation of the bending moment in the bar, $M_b^{(1)}$, is simply given by

$$M_b^{(1)} = F \times b \tag{13}$$

This bending moment M_b must result in a deflection with the maximum displacement δ in the notch region that is proportional to the moment and inversely proportional to Young's modulus E. Due to this displacement an additional moment ΔM_b is generated, Fig. 8d.

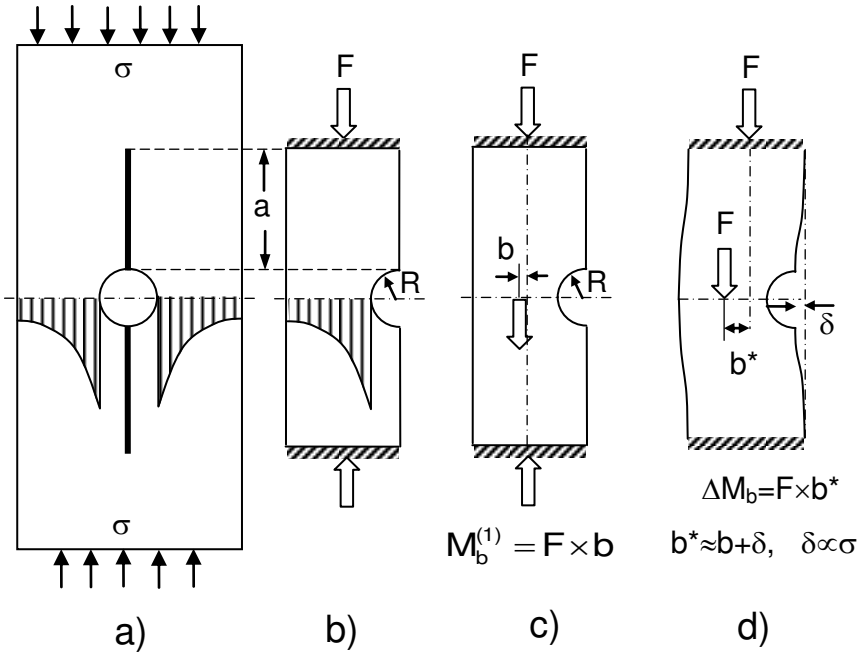

Fig. 8 Bending moment in a half of a DCDC-specimen that contributes to the stress intensity factor, a) full specimen with stress distribution, b) left half of the specimen with reduced length of a and rigidly clamped ends, c) compressive stresses replaced by the resultant acting parallel to the length axis in distance b, d) increased moment due to the displacement δ.

The displacement δ is available from FE-computations by He et al. [1]. Figure 9 shows results of COD at the crack mouth. The curves in Fig. 9 can be approximated for a/R>4 by straight lines that we fitted by the relation

$$\delta \cong 25.6 \left(\frac{H}{R}\right)^{-2.29} \frac{\sigma}{E} a \tag{14}$$

appropriate for $2.5 \le H/R$. Consequently, the bending moment, M_b, and the stress intensity factor, $K \propto M_b$, are

$$K \propto M_b \cong F \times (b + \delta) \propto \sigma \times (b + \alpha\sigma) \tag{15}$$

with a numerical coefficient α replacing the proportionality of eq.(14). Equation (15) makes clear that K is no longer linear for large values of σ/E, i.e. for large a/R. This effect is visible in some of the curves in Fig. 5 at about $a/R > 8$.

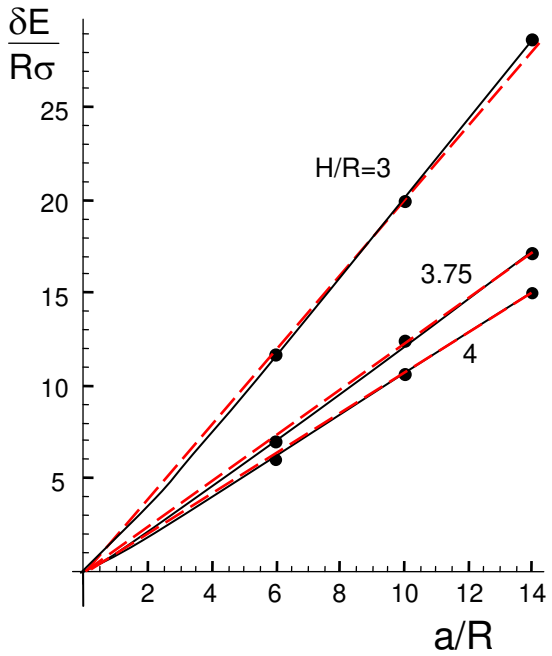

Fig. 9 COD at the crack origin as a function of crack length.

Conclusions:

- The 2-dimensional K-solutions from literature, obtained on the basis of 2-dimensional FE computations, do not sufficiently describe the real 3D-problem.
- The slopes of the normalized reciprocal stress intensity factor, Fig. 5, depend obviously on the Poisson's ratio ν.
- For the computation of stress intensity factors for DCDC-tests, the effect of deviating slopes in the load vs. crack length curves should be included.
- Since nonlinearities for large cracks occur, the evaluation including only a linear dependency of a/R should be limited by $a/R < 8$.

References

1 He, M.Y., Turner, M.R., Evans, A.G., Analysis of the double cleavage drilled compression specimen for interface fracture energy measurements over a range of mode mixities, Acta metall. mater. **43**(1995), 3453-3458.

2 Lardner, T.J., Chakravarthy, S., Quinn, J.D., Ritter, J.E., Further analysis of the DCDC specimen with an offset hole, Int. J. Fract. **109**(2001), 227-237.

3 Fett, T., Stress intensity factors, T-stresses, Weight functions, IKM 50, Universitätsverlag Karlsruhe, 2008.

4 G. Pallares, L. Ponson, A. Grimaldi, M. George, G. Prevot, M. Ciccotti, Crack opening profile in DCDC specimen, Int. J. Fract. **156**(2009), 11-20.

5 T.A. Plaisted, A.V. Amirkhizi, S. Nemat-Nasser, Compression-induced axial crack propagation in DCDC polymer samples: Experiments and Modeling, Int. J. Fract. 141(2006), 447-457.

6 C. Nielsen, A. V. Amirkhizi, S. Nemat-Nasser, The effect of geometry on fracture strength measurement using DCDC samples, Engng. Fract. Mech. **91**(2012) 1–13.

7 Fett, T., Fünfschilling, S., Hoffmann, M.J., Oberacker, R., Jelitto, H., Schneider, G.A., R-curve determination for the initial stage of crack extension in Si_3N_4, J. Am. Ceram. Soc., **91**(2008), 3638-42.

8 Fünfschilling, S., Fett, T., Hoffmann, M.J., Oberacker, R., Jelitto, H., Schneider, G.A., Determination of the crack-tip toughness in silicon nitride ceramics, J. Mater. Sci. Letters, **44**(2009), 335-338.

9 H. Cai, K.T. Faber, E.R. Fuller, Crack bridging by inclined fibers/whiskers in ceramic composites, J. Am. Ceram.Soc. **75**(1992), 3111-3117.

10 T.A. Michalske, W.L. Smith, E.P. Chen, Stress intensity calibration for the double cleavage drilled compression specimen, Engng. Fract. Mech., **45**(1993), 637-642.

11 K.G. Schell, S. Wagner, P. Hettich, T. Fett, G. Rizzi, M.J. Hoffmann, Identification of residual stress layers at glass surfaces via crack terminating angles, J. Am. Ceram. Soc. **100**(2017), 4173-79.

KIT Scientific Working Papers
ISSN 2194-1629

www.kit.edu